ATMOSPHERIC SCIENCE LETTERS
*Atmos. Sci. Let.* **18**: 19–28 (2017)
Published online in Wiley Online Library
(wileyonlinelibrary.com) **DOI:** 10.1002/asl.719

RMetS
Royal Meteorological Society

# Empirical and modeling analyses of the circulation influences on California precipitation deficits

Yen-Heng Lin,[1]* Lawrence E. Hipps,[1] S.-Y. Simon Wang[1,2] and Jin-Ho Yoon[3]

[1]*Department of Plants, Soils and Climate, Utah State University, Logan, UT, USA*
[2]*Utah Climate Center, Utah State University, Logan, UT, USA*
[3]*School of Earth Sciences and Environmental Engineering, Gwangju Institute of Science and Technology, South Korea*

**Correspondence to:*
*Y.-H. Lin, Department of Plants, Soils and Climate, Utah State University, 4820 Old Main Hill, Logan, UT, USA.*
*E-mail: yheng@pie.com.tw*

Received: 20 April 2016
Revised: 7 October 2016
Accepted: 10 November 2016

## Abstract

**Amplified and persistent ridges in western North America are recurring features associated with drought conditions in California. The recent drought event (2012–2016) lasted through both La Niña and El Niño episodes, suggesting additional climate drivers are important in addition to the commonly perceived El Niño-Southern Oscillation. Diagnostic analyses presented here suggest that, while the Pacific North American (PNA) and North Pacific Oscillation (NPO) do not directly cause drought in California, the relationships between them and with the upper air circulation pattern do modulate the spatial drought pattern. The positive PNA relative circulation leads drier northern California, and (-NPO) relative circulation leads southern California to be drier. The types of drought in this region emerge mostly from the combination of two PNA and NPO relative oceanic and atmospheric oscillations. At present, climate model projections do not indicate any significant change in these particular drought-modulating processes.**

**Keywords:** **California drought; circulation type; drought variation**

## 1. Introduction

During the winters from 2011–2012 to 2014–2015, a persistent upper tropospheric ridge developed over the Northeastern Pacific, and this anomalous ridge prohibited much of the rain-producing weather disturbances from reaching California. The reduction in the rainy-season precipitation and warmer temperature led to a major drought with declined snowpack and subsequently less water during the dry seasons. While the occurrence of drought is not uncommon in California (Department of Water Resources, 1978, 1993, 2015), the fact that this recent drought episode has lasted four consecutive years was unprecedented in a 1200-year reconstructed history (Robeson, 2015).

Various climate modes impact the winter precipitation in California, such as the North Pacific Oscillation (NPO) or West Pacific (Linkin and Nigam, 2008), the Pacific North American (PNA; Renwick and Wallace, 1996), and the El Niño-Southern Oscillation (ENSO) patterns. Even though California droughts are closely associated with an amplified and stagnant ridge over the western United States, the formation mechanism of the ridge itself is elusive (Wang *et al.*, 2014), and the interpretation of the causes of historical droughts in California has been inconsistent. The notable 1976–1977 California drought winter was reported to associate with the El Niño (Namias, 1978). However, this was contradicted by the argument of Seager *et al.* (2015) that the 2012 California drought was initiated by the 2011 La Niña. Apart from the classic view that ENSO and the Pacific Decadal Oscillation collectively contribute to California's dry winters (McCabe and Dettinger, 1999; Kam *et al.*, 2014), recent studies that focused on the post-2012 drought identified other unique atmospheric and oceanic features. For example, Wang and Schubert (2014) suggested that the 2013 sea surface temperature (SST) anomalies in the North Pacific produced a predilection for the ensuing California drought. Swain *et al.* (2014) pointed out the record-setting ridge in the upper troposphere as the cause of drought, while Wang *et al.* (2014) reported the associated geopotential height dipole (with a trough counterpart over the Great Lakes) was linked to an ENSO precursor. Subsequent studies (Hartmann, 2015; Lee *et al.*, 2015) also linked the 2013–2014 SST pattern to the North Pacific Mode (Deser and Blackmon, 1995) with an amplitude modulation from reduced sea ice content in the Arctic.

How do we reconcile these different observations and interpretations about which climatic features and variability influence drought conditions in California? In addressing this question, we shifted our attention on the atmospheric circulation and SST settings that affect *the pattern of drought*. The hypothesis addressed is that there are different dynamical processes that govern events leading to several distinct patterns of drought. This differs from previous studies searching for simply the causes of drought, implying that all droughts are the same. Additional understanding of the different types of atmospheric patterns associated with patterns of dry episodes could help society anticipate or mitigate the next drought.

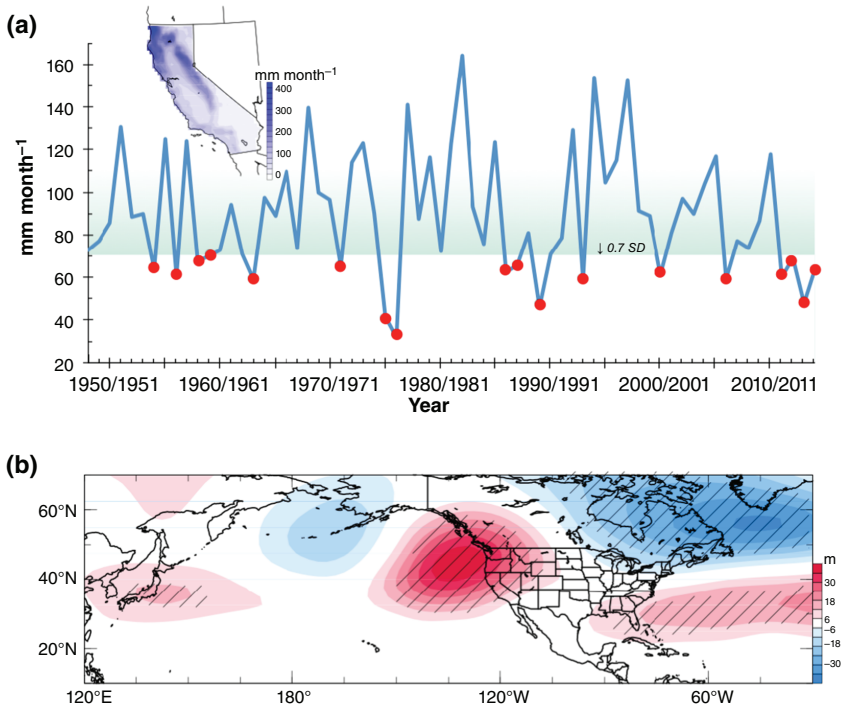


**Figure 1.** (a) Winter season (November–March) precipitation time series over California; the inset map shows the domain and winter mean precipitation in California. The red dots indicate the 18 dry winters in which precipitation was <0.7 standard deviation below average as shaded. (b) The composite anomaly of the 250-hPa geopotential height of the 18 drought winters. Hatches indicate significant level at $p < 0.05$ for the anomaly.

## 2. Data

To depict the winter season from November to March precipitation deficit over California, we utilized the parameter-elevation regressions on independent slopes model (PRISM) (Daly *et al.*, 2008) precipitation at 4 km horizontal resolution developed by Oregon State University (http://prism.oregonstate.edu). For the atmospheric circulation, we analyzed the monthly National Centers for Environmental Prediction (NCEP)/National Center for Atmospheric Research (NCAR) reanalysis data with a spatial resolution of 2.5° × 2.5° from 1948 to 2015 (Kalnay *et al.*, 1996). To explore the SST pattern, we analyzed the monthly NOAA extended reconstructed SST version 3 with a 2° × 2° spatial resolution (Smith *et al.*, 2008). For the purpose of documenting the drought connection to climate patterns, we also examined existing climate indices archived by the National Oceanic and Atmospheric Administration (NOAA) earth system research laboratory: http://www.esrl.noaa.gov/psd/data/climateindices/list/. Owing to the maximum extent of NCEP datasets, the analysis period of observational data is from 1948 to 2015. To reveal the drought distribution, the PRISM-derived Palmer Drought Severity Index (PDSI) (Palmer, 1965) data with 4 km horizontal resolution were also utilized. The PDSI is constructed by taking into account water supply, water demand, and soil moisture information influenced by surface temperature, and is used commonly to show the global and regional drought features (Heim, 2002; Dai *et al.*, 2004).

To further examine the variations of climate variability under external climate forcing and understand long-term changes, the historical and future simulations of Community Earth System Model version 1 (CESM1) (Hurrell *et al.*, 2013) with Community Atmosphere Model version 5.0 (CAM5) for the atmospheric component were used. The model version and setting follow Yoon *et al.* (2015a). Thirty ensemble members of CESM1 with 0.9° × 1.25° horizontal resolution through the large-ensemble project (Kay *et al.*, 2015) were utilized. The historical forcing scenario (HIS run), including greenhouse gases, aerosols, volcanic activity, ozone, land use change, and solar, covers 1920–2005 period, and the future Representative Concentration Pathway (RCP) 8.5 forcing scenario (RCP run) that represents a high-emission pathway (Taylor *et al.*, 2012) covers 2006–2080 period. The climate indices, such as PNA and NPO, are computed by correlating the 250-hPa geopotential height onto corresponding PNA (0°E–360°E, 20°N–90°N) and NPO (165°E–90°W, 10°N–70°N) loading patterns during the winter season in each ensemble. The loading patterns are generated by regressing NCEP's 250-hPa geopotential height onto observational PNA and NPO indices. The ensemble spread of initial conditions is generated by the 'round-off differences' method (Kay *et al.*, 2015).

## 3. Results

To understand the circulation variations in drought years in California, we first identify precipitation deficit

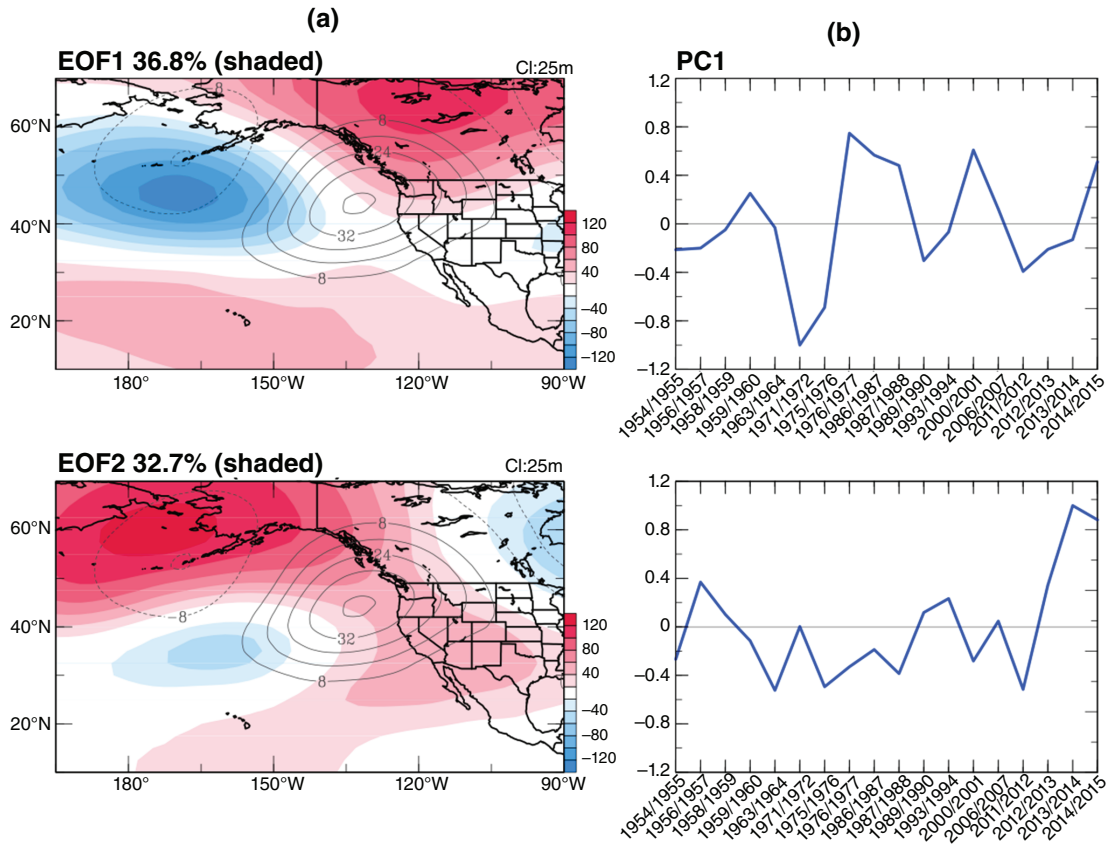


**Figure 2.** (a) The first two leading EOFs (shaded) of winter season (November–March) $Z_{250}$ within the 18 dry winters, superimposed with their composite $Z_{250}$ anomalies (contour). (b) The corresponding PCs in relation to each of the 18 dry winters.

events. Based upon the winter (November–March) precipitation in California ($P_{CA}$), which is shown in Figure 1(a) from 1948–1949 to 2014–2015, we defined the occurrence of drought to be when $P_{CA}$ exceeded 0.7 standard deviation below the 57 years winter mean, a threshold to balance water deficit intensity with a sufficient number of cases. This definition of drought led to the inclusion of recent severe droughts of 1976–1977, 2011–2012, and 2014–2015, as well as other major low-precipitation years, isolating 18 drought events as indicated by red dots. Figure 1(b) shows the composite 250-hPa geopotential height anomalies of these 18 drought winters (as a departure from the 1948–2015 mean), depicting a prominent high-pressure anomaly centered off Northwestern United States and western Canada, but covering much of the western United States including California. Such a ridge will prohibit the occurrence of winter storms that produce rainfall in California (Swain *et al.*, 2014). A discernible yet weak wave train emerges in the upstream region over the North Pacific. Given its upstream source near the western North Pacific, this wave train appears to be different from the ENSO-induced teleconnection forced by the central/eastern tropical Pacific heating anomalies (Schonher and Nicholson, 1989). Another notable feature in the downstream side over northeastern North America is a robust anomalous trough that, together with the western ridge, forms the so-called North American dipole (Wang *et al.*, 2015).

To analyze the extent to which these 18 droughts differ case-to-case, we first applied the empirical orthogonal function (EOF) to depict the variation of the November–March 250-hPa geopotential height ($Z_{250}$) within these 18 drought events. The analysis here was focused on the region encompassing the composite ridge anomaly (165°E–90°W, 10°–70°N). The loading patterns of the first two leading modes (EOF 1 and 2) are shown in Figure 2(a) as shadings, which are superimposed on composite $Z_{250}$ contours for comparison. These two EOFs constitute collectively about 70% of the total variance, meaning that the first two leading modes are the major circulation variations. It is noteworthy that they are also about the same fraction of variance, and thus importance. EOF1 depicts a northeastern extension of the anomalous ridge in the positive phase (according to the principal component or PC; Figure 2(b)) and a westward extension over the Gulf of Alaska in the negative phase. In EOF2, the anomalous ridge would expand mostly toward the northwest of the Bering Sea and into the southwestern United States as well. This pattern has shown prominence during the recent (2013–2014) drought as noted by Wang *et al.* (2014). Similar results are revealed in the upper troposphere at 200 and 500 hPa, as shown in Figure S1. These results are empirical evidence of the existence of two distinct climate circulation schemes that affect the pattern of drought in this region.

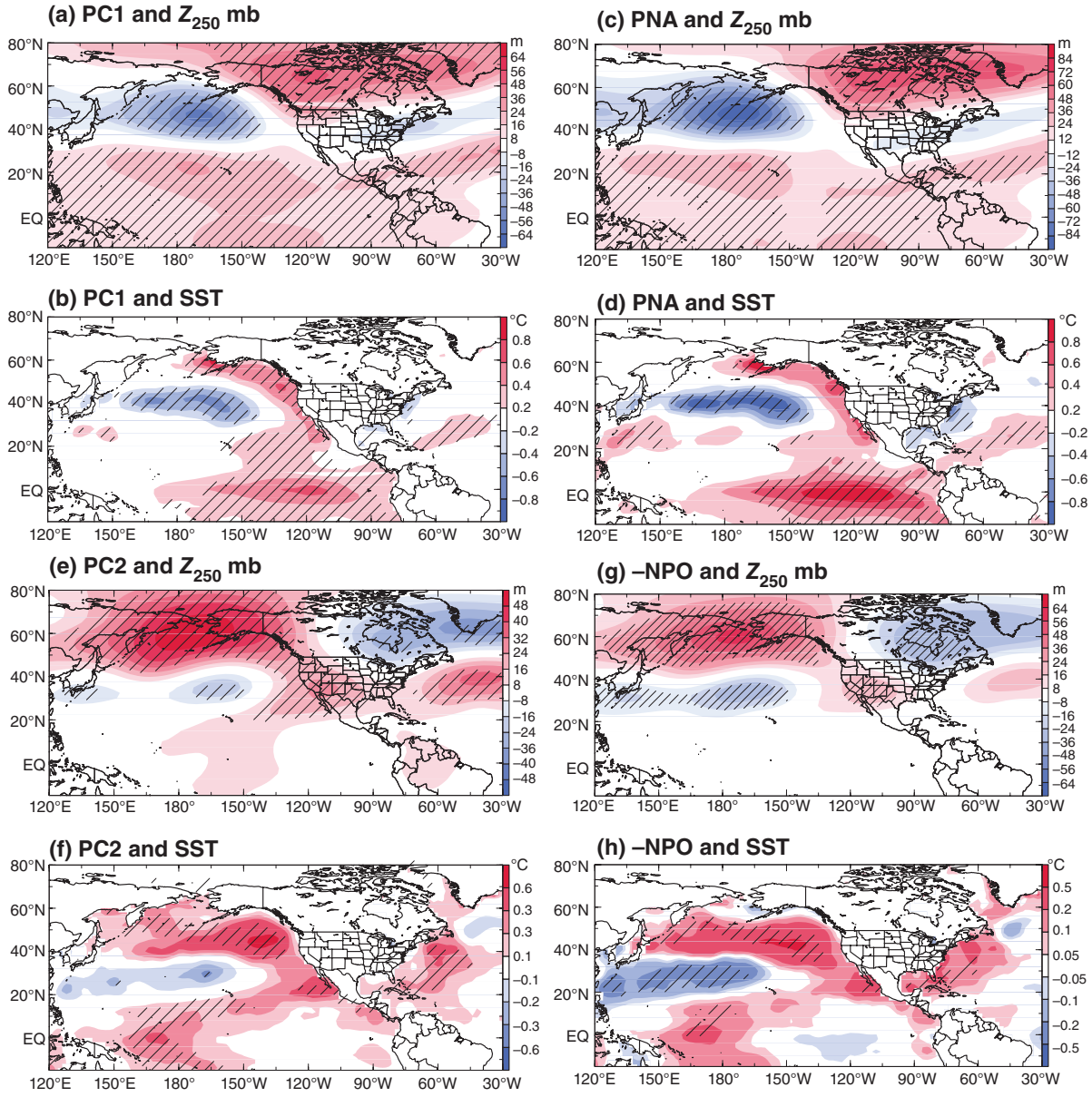


**Figure 3.** The $Z_{250}$ and SST patterns from the 18 California dry winters regressed upon PC1 (a and b), PNA index (c and d), PC2 (e and f), and −NPO index (g and h). Hatches indicate significant level at $p < 0.05$ for the regression.

The intensity of these two EOFs was proportional to the amplitude of the PC values. Therefore, we correlated the PC of 18 drought winters with different climate indices of the same 18 drought winters; these correlation coefficients are summarized in Table S1, Supporting information. The results illustrate that PC1 has a high positive correlation ($r = 0.90$) with the PNA index (Barnston and Livezey, 1987), while PC2 has a high negative correlation ($r = -0.83$) with the NPO. The NPO is a leading atmospheric variation mode determined as the second PC of the November–March 1000-hPa height anomalies over North Pacific (Rogers, 1981). Similarly, the linear regression patterns of $Z_{250}$ with PC1 (Figure 3(a)) and PNA (Figure 3(c)) for the 18 dry winters appear to be similar, while the corresponding SST regressions (Figures 3(b) and (d)) reveal an ENSO-like pattern. This is not surprising since ENSO is the prime forcing of the PNA teleconnection (Yu and Zwiers, 2007), even though ENSO does not connect as prominently to the PC series of $Z_{250}$ (Table S1). Meanwhile, the height and SST regression patterns with PC2 (Figure 3(e)) and −NPO (Figure 3(g)) both present a distinct high-latitude seesaw from the Tropics to the Bering Sea and its associated 'triband' SST anomalies (Figures 3(f) and (h)) as noted by Linkin and Nigam (2008). We note that the NPO's associated SST pattern (Figure 3(h)) is also similar to the 'North Pacific Mode' of SST identified by Deser and Blackmon (1995), which depicts the SST counterpart of the sea level pressure-based NPO. Given that PNA and NPO represent atmospheric modes, there may be intra-seasonal variability that is overlooked in this seasonal mean analysis.

The results shown in Figure 3 suggest that different climate forcing sources may influence the distribution and intensity of droughts by modulating

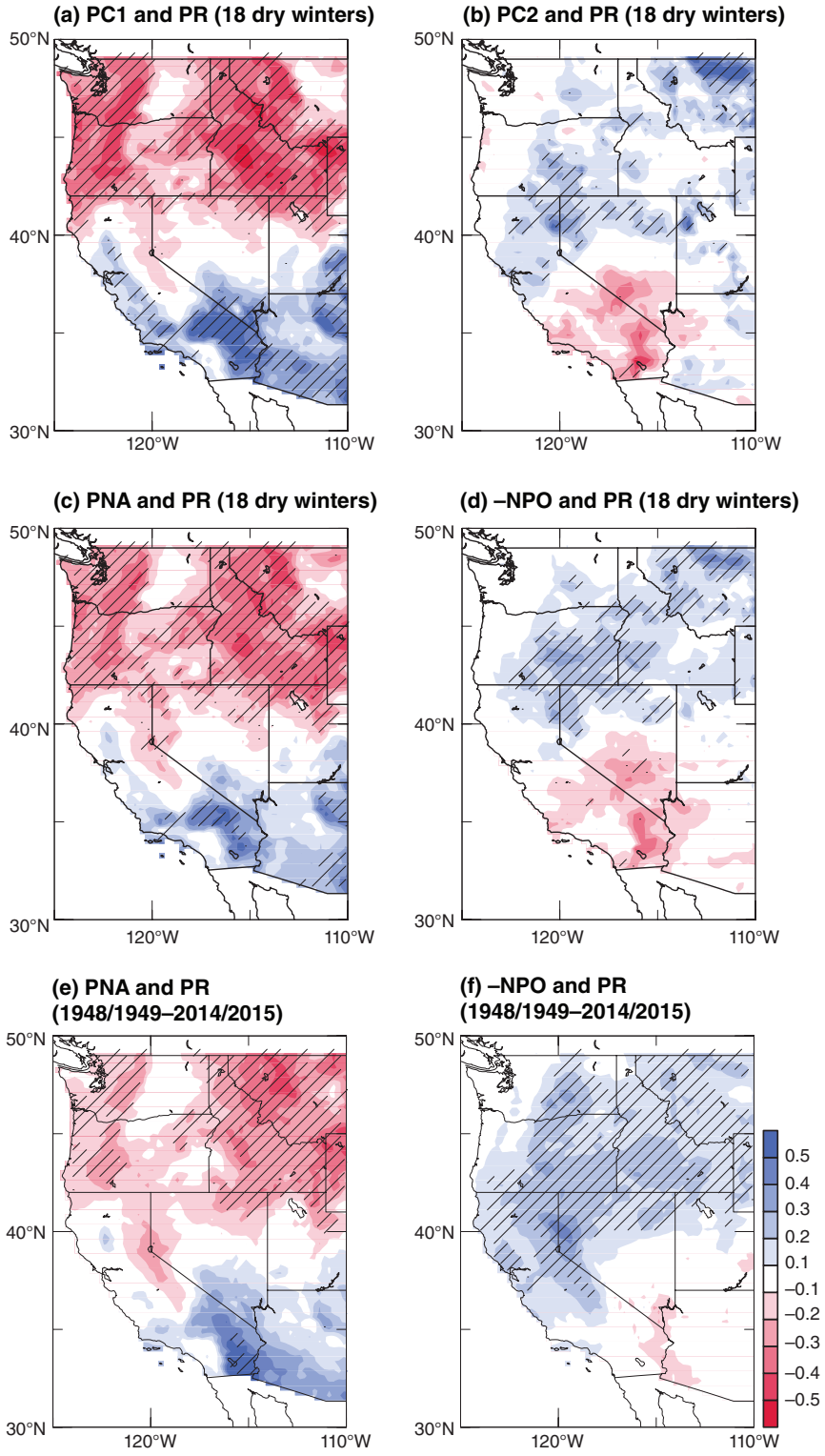


**Figure 4.** The influence ratio from the regression of 18 drought years precipitation onto (a) PC1, (b) PC2, (c) PNA, and (d) –NPO decided by the mean precipitation anomaly during drought years. (e) and (f) are the same as (c) and (d) but for 1948/1949–2014/2015 wintertime precipitation.

the drought-inducing ridge. To examine these teleconnection impacts on the drought pattern, we show in Figures 4(a) and (c) the association of PC1 and PNA with precipitation in the drought winters. Here, the values represent influence ratio on precipitation that is calculated from the regressions of precipitation onto each normalized index divided by the mean precipitation anomaly within the 18 dry winters, ranging between −1 and 1. Positive cases of PC1 and PNA are associated with drier conditions in the Pacific Northwest, leaking into northern California, and less dry conditions in southern California and western/southwest coast of California. This shift of drought pattern is caused by the anomalous ridge being

extended further northeastward (EOF1; Figure 2(a)). For PC2 and the −NPO, impacts on precipitation (Figures 4(b) and (d)), southern California and some of the Southwest United States experience more severe drought conditions, and correspondingly northern California and some of Northwest United States exhibit less intense drought with the southward extension of the high-pressure ridge (EOF2; Figure 2(a)). Although the influence fractions of PNA and NPO on California drought winters' precipitation do not show big differences (about 10–20%) in Sierra Nevada, the connections are larger in the coastal and agriculture intensive (valley) regions (Figures 4(b) and (d)). Moreover, it is instructive to consider that drought may not be defined only by precipitation. The regression results of PDSI in drought winter onto PC1/PNA and PC2/(−NPO) (Figures S3(a)–(d)) show the PNA and NPO are related to a measure of drought intensity, especially in southern California, with changes of over 1 point of PDSI value.

It appears that both the PNA and NPO, in addition to ENSO, modulate the drought pattern in California, as well as the western United States, but they do not directly cause the drought (i.e. due to their weak direct relationship with precipitation in California). This latter point is demonstrated in Figures 4(e) and (f) showing the influence ratio on precipitation by regressing wintertime precipitation onto normalized PNA and NPO indices during the entire 1948–2015 period divided by the winter mean precipitation. It is clear that the patterns for the entire period (Figures 4(e) and (f)) resemble in general terms those of the 18 drought years (Figures 4(c) and (d)). The record low snowpack in the Sierra Nevada in 2013–2014 that was identified as the lowest in the past 500 years (Belmecheri *et al.*, 2016) coincided with a −PNA and a strong −NPO phases (Figure S2). This combined influence on the extreme low snowpack further intensified the drought making it harder to recover. However, even though the precipitation pattern bears resemblance with the variations within the 18 drought winters, neither the PNA nor NPO shows statistically significant correlations with precipitation within California. A similar lack of correlation was also found between the PNA/NPO and the winter PDSI (Figure S3). Altogether, these results suggest that the PNA and NPO play more of a modulating role of drought in California rather than causing it.

Further validation was carried out by analyzing the CESM1 large-ensemble simulations of HIS and RCP runs. By applying the same analysis as in the observational data, the simulated geopotential height anomalies in each of the 30 members reveal similar PNA and NPO features, both in the leading EOFs and regression patterns. In Figure S4, we show the ensemble mean of PNA-like and NPO-like EOFs of each scenario. The results show that the HIS and RCP runs have similar variances in the first two leading modes, suggesting that the CESM1 simulations agree that PNA and NPO are key circulation features that modulate the drought pattern in California. Figures S5 and S6 show the averaged regression patterns of each ensemble's PC onto CESM1's $Z_{250}$ and SST, suggesting that the influence of modeled PNA (NPO) on California droughts slightly increase (decrease) in RCP run. Recent studies (Zhou *et al.*, 2014; Yoon *et al.*, 2015a) have indicated that the anthropogenic warming would change North Pacific circulation and, in turn, would influence climate conditions in North America. The result from CESM1's RCP run suggests that this influence would be realized through the modulations of PNA and NPO.

## 4. Discussions

The PNA and NPO relative circulations are associated with the spatial distribution of precipitation during drought in California. Meanwhile, when applying the EOF analysis on the 18 drought winters' standardized normalized precipitation over California region (Figures S7(a) and (b)), the first two leading modes also have about 70% of total variance, which is similar with the EOF analysis of $Z_{250}$ hPa. However, the first mode of EOF for precipitation shows no distinct spatial pattern, while the second mode does show a strong north–south pattern. The correlation patterns of $Z_{250}$ hPa onto two leading PCs for precipitation do not show any significant correlation coefficients (at $p < 0.05$ level) (Figure S7(c)). It means these two orthonormal eigenvectors are not associated with a specific circulation pattern.

If one looks more closely, the first mode of EOF for the 18-drought winters precipitation is associated with the first and second EOFs of $Z_{250}$ hPa being opposite in sign (Figure 2). Recall the value of the first mode of $Z_{250}$ hPa is associated with the PNA, and the value of the second is associated with −NPO. Since the regressions of PNA and −NPO with precipitation have opposite dipole patterns near California (Figures 4(c) and (d)), the result is that the two regressions effectively counter each other and no dipole pattern is observed. So the first mode of precipitation is associated with PNA and −NPO having the same sign, it displays no spatial pattern. In contrast, the second leading mode of EOF for California 18-drought winters precipitation appears to result from a constructive effect of PNA and −NPO (Figures 4(c) and (d)) to enhance the dipole pattern. This is because, in this case the PC1 and PC2 of the $Z_{250}$ hPa, associated with PNA and −NPO, have opposite signs, so the respective regressions with precipitation have similar spatial patterns, that re-enforce each other. Therefore, it is the combination of the signs of the circulation EOFs, related to those of the PNA and −NPO that relate to spatial patterns of drought year precipitation, and several types of droughts in California.

The forcing sources of the PNA are manifold, and previous studies have indicated that the intensity of the PNA is associated with the eastern tropical Pacific SST (Straus and Shukla, 2002; Yu and Zwiers, 2007) and the East Asian Jet Stream (Wallace and Gutzler, 1981; Leathers and Palecki, 1992). This explains the second highest correlation coefficient of the Niño indices with

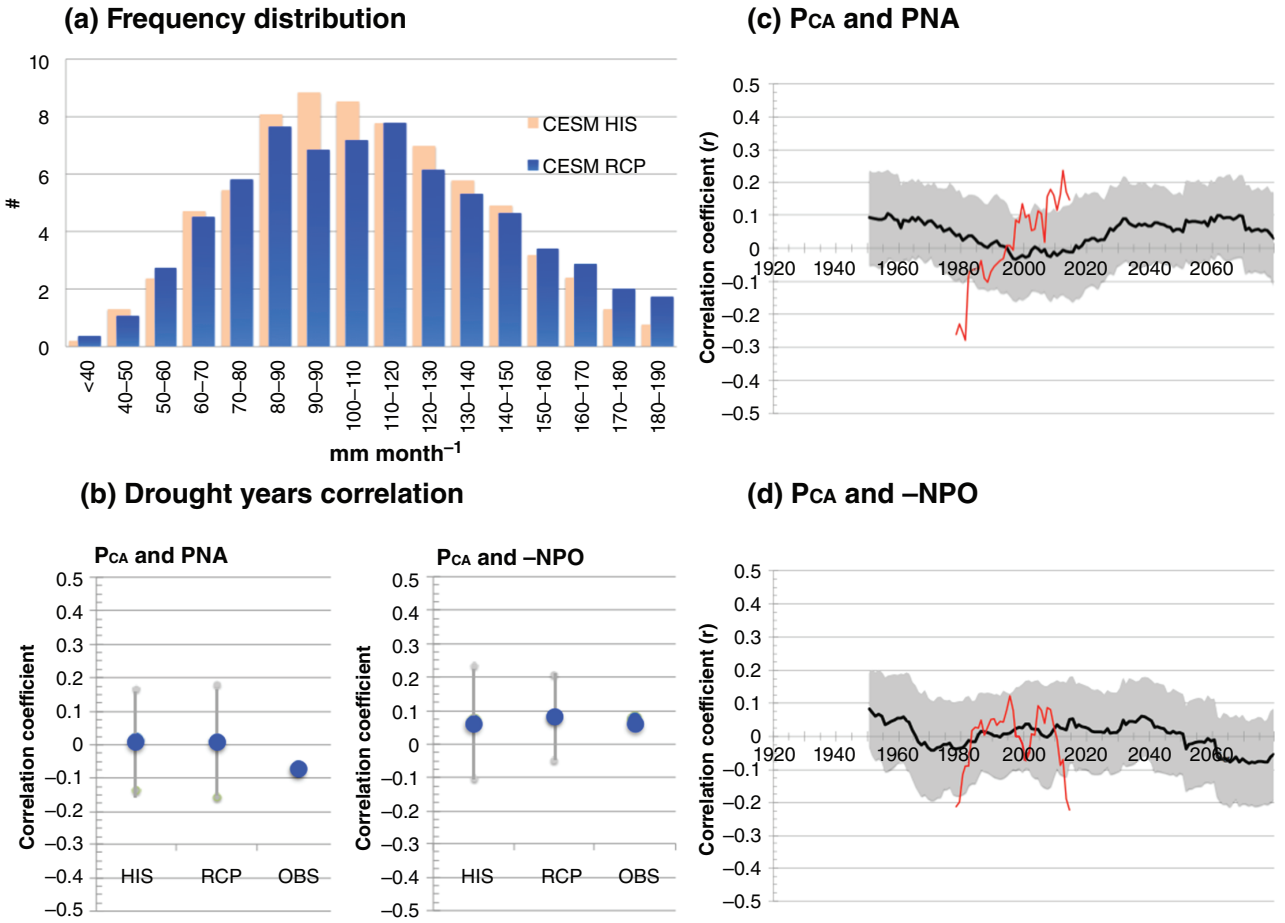


**Figure 5.** The precipitation changes in California simulated by CESM1 with 30 ensembles. (a) The ensemble mean of frequency distribution of November–March precipitation in California ($P_{CA}$). The historical scenario (HIS run) includes 74 years before 2005, and the RCP 8.5 scenario (RCP run) includes 74 years after 2005. (b) The correlation coefficient between $P_{CA}$ and PNA (left) and between $P_{CA}$ and –NPO (right) within drought years on ensembles' HIS/RCP runs and observational data (OBS). The blue circles show the correlation coefficient of ensemble mean or observation, and the gray bar indicates 50% of ensemble spread. (c) The 30-year window sliding correlation between PNA and $P_{CA}$ over simulation period. The black solid line is the ensemble mean, the shaded areas indicate 50% of ensemble spread, and the red line is the observational data. (d) The same as (c) but for $P_{CA}$ and –NPO.

PC1 as shown in Table S1. The NPO's role in the modulation of the California drought does connect to ENSO, since the NPO acts as an ENSO precursor (i.e. no direct correlation) through interactions with tropical SST and wind anomalies across the equatorial Pacific. The NPO's role in triggering ENSO occurs under the so-called 'Seasonal Footprinting Mechanism', from which the NPO imparts a surface wind stress to change the surface heat fluxes and underlying SST (Vimont *et al.*, 2003; Alexander *et al.*, 2010). These features supplement the common perception that ENSO and its different phases are responsible for California drought. Recent studies (Yoon *et al.*, 2015a, 2015b) projected that both intense drought and excessive flooding in California may increase by 50% toward the end of the 21st century, and this projection is based upon a strengthened relation to the ENSO cycle, not only through its warm and cold phases but also through its precursor (transition) patterns.

The long-term precipitation regression results with PNA and NPO indices from 1948–1949 to 2014–2015 show much less significance than the relationship of variations within California (Figures 4(e) and (f)). For example, the winters of 1975–1976 and 1976–1977 were associated with a distinct opposite phase of the PNA pattern and El Niño SST anomalies, while in 2011–2012 a La Niña SST pattern prevailed. The recent record droughts in 2013–2014 and 2014–2015 were associated with an amplified NPO (Figure 2(b)) without the presence of a mature-phase El Niño. The lack of association between the California drought and the PNA and the NPO is evident in Figure S2 indicating a mixture of phases in either index during the 18 dry winters. These reported features and the association with the NPO make simulation and/or prediction for California's winter climate difficult, since the majority of models do not simulate the ENSO precursors (i.e. the NPO) so well (Wang *et al.*, 2015; Yoon *et al.*, 2015a). Further research is needed in identifying the source of variability and predictability in the drought-producing ridge off the Northwest United States region as revealed in Figure 1(b).

Analysis of the CESM1 large-ensemble simulations with historical and RCP forcing scenarios is supportive

of the respective roles of PNA and NPO in modulating the drought pattern. This finding led us to question the extent to which the relations between PNA/NPO and California's precipitation may change in the future climate. To answer this question, Figure 5(a) shows the frequency distribution of California winter precipitation superimposed with the CESM1's simulations. While the HIS run presents a normal distribution, the RCP run shifts the wet tail substantially and the dry tail slightly (far left). These results are consistent with the finding of the increased water cycle extremes in California projected by Yoon *et al.* (2015a), although the annual precipitation may not change with human-induced climate change (Pierce *et al.*, 2013). Furthermore, the correlation coefficients of PNA/NPO and California precipitation within the drought winters (Figure 5(b)) and the sliding correlation coefficients of PNA/NPO and California precipitation with a 30-year window over all simulation period (Figures 5(c) and (d)) both show that, despite of the projected change in the frequency distribution of California precipitation, its association with either PNA or NPO remains very weakly and insignificantly correlated.

## 5. Conclusions

The upper-atmospheric high-pressure (ridge) anomaly that accompanies drought in California exhibits several patterns, which modulates the spatial distribution of precipitation during drought in this region. These findings suggest that the variations of the ridge are collectively *modulated* – but *not directly caused* – by a combination of geopotential heights, and the synchronization of the signs of the PNA and NPO. Neither the PNA nor the NPO appears to directly contribute to the formation of drought, at least for the winter season. Rather, they alter the pattern of drought. There are several different combinations of forcing factors ($Z_{250}$ hPa, PNA, and NPO) that are associated with drought in California.

The analysis of CESM1 simulations indicates that these modulations of PNA and NPO will not change significantly in the future, although there is a projected increase in the extreme wet/dry anomalies in California.

In terms of future research, a couple of unsolved questions are worth pursuing: (1) investigating whether the appearance of drought-producing ridge anomaly is actually forced or caused by any prominent mode of climate variability, or is purely due to random changes in atmospheric states, and (2) examining the impacts of constructive and destructive superposition of the PNA and NPO and how well they can be simulated in seasonal predictions. Lastly, even though this study is focused on precipitation, the effect of temperature on exacerbating drought cannot be discounted; this temperature effect was recently demonstrated using paleoclimate record for the California drought (Griffin and Anchukaitis, 2014). The effect of anthropogenic warming as suggested by recent studies on the increasing chances of low-precipitation years in California (AghaKouchak *et al.*, 2014; Diffenbaugh *et al.*, 2015; Yoon *et al.*, 2015a) and the associated dynamic processes warrants further investigation.

### Acknowledgements

This research was supported by the Utah Agricultural Experiment Station, Utah State University (journal paper number 8951), and the Utah State University Libraries Open Access Fund. Yen-Heng Lin is supported by the Utah State University Presidential Doctoral Research Fellows (PDRF) program. JHYoon is supported by the Korea Meteorological Administration Research and Development Program under Grant KMIPA 2016-6030. The reanalysis data is provided by the NOAA/OAR/ESRL PSD, Boulder, Colorado, USA, from their Web site at http://www.esrl.noaa.gov/psd/.

## Supporting information

The following supporting information is available:

**Table S1**. The correlation results between PCs and winter mean (November–March) of climate index over 18 California dry winters. The highest corollary/anticorollary index with PC1 or PC2 is shaded.

**Figure S1**. The same as Figure 2, the first two leading EOFs (shaded) and PCs of winter (November–March) geopotential height ($Z$) within the 18 dry winters, superimposed with dry winters' $Z$ anomalies (contour), but for (a) $Z_{200}$ hPa and (b) $Z_{500}$ hPa.

**Figure S2**. Winter season (November–March) precipitation in California (blue line) overlaid with (a) the PNA index (orange line) and (b) the inverted NPO index (pink line) from 1948–1949 to 2014–2015, superimposed with the 18 dry winters as vertically shaded.

**Figure S3**. (a)–(d) Same as Figure 3 but for the regression patterns of the PDSI with the PNA and NPO indices. (e) and (f) Long-term regressions of the PDSI with the PNA and the inverted NPO over the 1948–2015 period. Hatches indicate significant level at $p < 0.05$ for the regression.

**Figure S4**. The 30 ensembles mean of the EOF analysis of 250-hPa HGT from each ensemble's drought years. (a) The PNA-like EOFs of HIS run, (b) the −NPO-like EOFs of HIS run, (c) the PNA-like EOFs of RCP run, and (d) the −NPO-like EOFs of RCP run. The contour shows the drought years' anomaly in HIS run (a and b) and RCP run (c and d).

**Figure S5**. Averaged $Z_{250}$ hPa regression patterns from 30 ensembles in drought years by regressing with the PCs of (a) PNA-like EOFs from HIS run, (b) −NPO-like EOFs from HIS run, (c) PNA-like EOFs from RCP run, and (d) −NPO-like EOFs from RCP run.

**Figure S6**. Averaged SST regression patterns from 30 ensembles in drought years by regressing with the PCs of (a) PNA-like EOFs from HIS run, (b) −NPO-like EOFs from HIS run, (c) PNA-like EOFs from RCP run, and (d) −NPO-like EOFs from RCP run.

**Figure S7**. (a) The first two leading EOFs of standardized normalized winter season (November–March) precipitation within the 18 dry winters over California, (b) the corresponding PCs in

relation to each of the 18 dry winters, and (c) the $Z_{250}$ patterns from the 18 California dry winters correlated upon PC1 and PC2 of California precipitation.

## References


AghaKouchak A, Cheng L, Mazdiyasni O, Farahmand A. 2014. Global warming and changes in risk of concurrent climate extremes: insights from the 2014 California drought. *Geophysical Research Letters* **41**: 8847–8852, doi: 10.1002/2014GL062308.

Alexander MA, Vimont DJ, Chang P, Scott JD. 2010. The impact of extratropical atmospheric variability on ENSO: testing the seasonal footprinting mechanism using coupled model experiments. *Journal of Climate* **23**: 2885–2901, doi: 10.1175/2010JCLI3205.1.

Barnston AG, Livezey RE. 1987. Classification, seasonality and persistence of low-frequency atmospheric circulation patterns. *Monthly Weather Review* **115**: 1083–1126.

Belmecheri S, Babst F, Wahl ER, Stahle DW, Trouet V. 2016. Multi-century evaluation of Sierra Nevada snowpack. *Nature Climate Change*, **6**: 2–3, doi: 10.1038/nclimate2809.

Dai A, Trenberth KE, Qian T. 2004. A global dataset of Palmer Drought Severity Index for 1870–2002: relationship with soil moisture and effects of surface warming. *Journal of Hydrometeorology* **5**: 1117–1130.

Daly C, Halbleib M, Smith JI, Gibson WP, Doggett MK, Taylor GH, Curtis J, Pasteris PP. 2008. Physiographically sensitive mapping of climatological temperature and precipitation across the conterminous United States. *International Journal of Climatology* **28**: 2031–2064, doi: 10.1002/joc.1688.

Department of Water Resources. 1978. *The 1976-1977 California Drought: A Review*. California Department of Water Resources, Sacramento, CA.

Department of Water Resources. 1993. *California's 1987-98 Drought: A Summary of Six Years of Drought*. California Department of Water Resources, Sacramento, CA.

Department of Water Resources. 2015. *California's Most Significant Droughts: Comparing Historical and Recent Conditions*. California Department of Water Resources, Sacramento, CA.

Deser C, Blackmon ML. 1995. On the relationship between tropical and North Pacific sea surface temperature variations. *Journal of Climate* **8**: 1677–1680, doi: 10.1175/1520-0442(1995)008, 1677:OTRBTA.2.0.CO;2.

Diffenbaugh NS, Swain DL, Touma D. 2015. Anthropogenic warming has increased drought risk in California. *Proceedings of the National Academy of Sciences of the United States of America* **112**: 3931–3936, doi: 10.1073/pnas.1422385112.

Griffin D, Anchukaitis KJ. 2014. How unusual is the 2012–2014 California drought? *Geophysical Research Letters* **41**: 9017–9023, doi: 10.1002/2014GL062433.

Hartmann DL. 2015. Pacific sea surface temperature and the winter of 2014. *Geophysical Research Letters* **42**: 1894–1902, doi: 10.1002/2015GL063083.

Heim RR Jr. 2002. A review of twentieth-century drought indices used in the United States. *Bulletin of the American Meteorological Society* **83**: 1149–1165.

Hurrell JW, Holland MM, Gent PR, Ghan S, Kay JE, Kushner PJ, Lamarque JF, Large WG, Lawrence D, Lindsay K, Lipscomb WH, Long MC, Mahowald N, Marsh DR, Neale RB, Rasch P, Vavrus S, Vertenstein M, Bader D, Collins WD, Hack JJ, Kiehl J, Marshall S. 2013. The community earth system model: a framework for collaborative research. *Bulletin of the American Meteorological Society* **94**(9): 1339–1360.

Kalnay E, Kanamitsu M, Kistler R, Collins W, Deaven D, Gandin L, Iredell M, Saha S, White G, Woollen J, Zhu Y, Leetmaa A, Reynolds R, Chelliah M, Ebisuzaki W, Higgins W, Janowiak I, Mo KC, Ropelewski C, Wang J, Jenne R, Joseph D. 1996. The NCEP/NCAR 40-year reanalysis project. *Bulletin of the American Meteorological Society* **77**(3): 437–471.

Kam J, Sheffield J, Wood EF. 2014. Changes in drought risk over the contiguous United States (1901-2012): the influence of the Pacific and Atlantic Oceans. *Geophysical Research Letters* **41**: 5897–5903, doi: 10.1002/2014GL060973.

Kay JE, Deser C, Phillips AS, Mai A, Hannay C, Strand G, Arblaster J, Bates S, Danabasoglu G, Edwards J, Holland M, Kushner P, Lamarque J-F, Lawrence D, Lindsay K, Middleton A, Munoz E, Neale R, Oleson K, Polvani L, Vertenstein M. 2015. The Community Earth System Model (CESM) large ensemble project: a community resource for studying climate change in the presence of internal climate variability. *Bulletin of the American Meteorological Society* **96**: 1333–1349, doi: 10.1175/BAMS-D-13-00255.1.

Leathers DJ, Palecki MA. 1992. The Pacific/North American teleconnection pattern and United States climate. Part II: temporal characteristics and index specification. *Journal of Climate* **5**: 707–716.

Lee M-Y, Hong C-C, Hsu H-H. 2015. Compounding effects of warm sea surface temperature and reduced sea ice on the extreme circulation over the extratropical North Pacific and North America during the 2013–2014 boreal winter. *Geophysical Research Letters* **42**: 1612–1618, doi: 10.1002/2014GL062956.

Linkin ME, Nigam S. 2008. The North Pacific Oscillation–West Pacific teleconnection pattern: mature-phase structure and winter impacts. *Journal of Climate* **21**: 1979–1997.

McCabe GJ, Dettinger MD. 1999. Decadal variations in the strength of ENSO teleconnections with precipitation in the western United States. *International Journal of Climatology* **19**(13): 1399–1410.

Namias J. 1978. Multiple causes of the North American abnormal winter 1976–77. *Monthly Weather Review* **106**: 279–295.

Palmer WC. 1965. Meteorological drought. Weather Bureau Research Paper 45, U.S. Department of Commerce, Washington, DC.

Pierce DW, Cayan DR, Das T, Maurer EP, Miller NL, Bao Y, Kanamitsu M, Yoshimura K, Snyder MA, Sloan LC, Franco G, Tyree M. 2013. The key role of heavy precipitation events in climate model disagreements of future annual precipitation changes in California. *Journal of Climate* **26**: 5879–5896, doi: 10.1175/JCLI-D-12-00766.1.

Renwick JA, Wallace JM. 1996. Relationships between North Pacific wintertime blocking, El Niño, and the PNA pattern. *Monthly Weather Review* **124**: 2071–2076.

Robeson SM. 2015. Revisiting the recent California drought as an extreme value. *Geophysical Research Letters* **42**: 6771–6779, doi: 10.1002/2015GL064593.

Rogers JC. 1981. The North Pacific Oscillation. *International Journal of Climatology* **1**: 39–57.

Schonher T, Nicholson SE. 1989. The relationship between California rainfall and ENSO events. *Journal of Climate* **2**: 1258–1269.

Seager R, Hoerling M, Schubert S, Wang H, Lyon B, Kumar A, Nakamura J, Henderson N. 2015. Causes of the 2011–14 California drought. *Journal of Climate* **28**: 6997–7024.

Smith TM, Reynolds RW, Peterson TC, Lawrimore J. 2008. Improvements to NOAA's historical merged land–ocean surface temperature analysis (1880–2006). *Journal of Climate* **21**: 2283–2296.

Straus DM, Shukla J. 2002. Does ENSO force the PNA? *Journal of Climate* **15**: 2340–2358.

Swain D, Tsiang M, Haughen M, Singh D, Charland A, Rajarthan B, Diffenbaugh NS. 2014. The extraordinary California drought of 2013/14: character, context and the role of climate change [in "Explaining Extremes of 2013 from a Climate Perspective"]. *Bulletin of the American Meteorological Society* **95**(9): S3–S6, doi: 10.1175/1520-0477-95.9.S1.1.

Taylor KE, Stouffer RJ, Meehl GA. 2012. An overview of CMIP5 and the experiment design. *Bulletin of the American Meteorological Society* **93**: 485–498, doi: 10.1175/BAMS-D-11-00094.1.

Vimont DJ, Wallace JM, Battisti DS. 2003. The seasonal footprinting mechanism in the Pacific: implications for ENSO. *Journal of Climate* **16**(16): 2668–2675.

Wallace JM, Gutzler DS. 1981. Teleconnections in the geopotential height field during the Northern Hemisphere winter. *Monthly Weather Review* **109**: 784–812.

Wang H, Schubert S. 2014. Causes of the extreme dry conditions over California during early 2013. *Bulletin of the American Meteorological Society* **95**(9): S7–S11.

Wang S-Y, Hipps L, Gillies RR, Yoon J-H. 2014. Probable causes of the abnormal ridge accompanying the 2013–2014 California drought: ENSO precursor and anthropogenic warming footprint. *Geophysical Research Letters* **41**: 3220–3226, doi: 10.1002/2014GL059748.

Wang S-YS, Huang W-R, Yoon J-H. 2015. The North American winter 'dipole' and extremes activity: a CMIP5 assessment. *Atmospheric Science Letters* **16**: 338–345, doi: 10.1002/asl2.565.

Yoon J-H, Wang S-Y, Gillies RR, Kravitz B, Hipps L, Rasch P. 2015a. Increasing water cycle extremes in California and in relation to ENSO cycle under global warming. *Nature Communications* **6**: 8657, doi: 10.1038/ncomms9657.

Yoon JH, Wang S-YS, Gillies RR, Hipps L, Kravitz B, Rasch PJ. 2015b. Extreme fire season in California: a glimpse into the future? *Bulletin of the American Meteorological Society* **96**: S5–S9, doi: 10.1175/BAMS-EEE_2014_ch2.1.

Yu B, Zwiers FW. 2007. The impact of combined ENSO and PDO on the PNA climate: a 1000-year climate modeling study. *Climate Dynamics* **29**: 837–851.

Zhou Z-Q, Xie S-P, Zheng X-T, Liu Q, Wang H. 2014. Global warming–induced changes in El Niño teleconnections over the North Pacific and North America. *Journal of Climate* **27**: 9050–9064, doi: 10.1175/JCLI-D-14-00254.1.